Taylor & Francis
healthsciences

Effects of Positioning Uncertainty and Breathing on Dose Delivery and Radiation Pneumonitis Prediction in Breast Cancer

Panayiotis Mavroidis, Sofie Axelsson, Simo Hyödynmaa, Juha Rajala, Maunu A. Pitkänen, Bengt K. Lind and Anders Brahme

From the Department of Medical Radiation Physics, Karolinska Institutet and Stockholm University, Stockholm, Sweden (P. Mavroidis, S. Axelsson, B.K. Lind, A. Brahme) and the Department of Oncology, Tampere University Hospital, Tampere, Finland (S. Hyödynmaa, J. Rajala, M.A. Pitkänen)

Correspondence to: Panayiotis Mavroidis, Department of Medical Radiation Physics, Karolinska Institutet and Stockholm University, P.O. Box 260, SE-171 76 Stockholm, Sweden. Tel: + 46 8 5177 2225. Fax: + 46 8 343 525. E-mail: takis@radfys.ks.se

Acta Oncologica Vol. 41, No. 5, pp. 471–485, 2002

The quality of the radiation therapy delivered in the treatment of breast cancer is susceptible to setup errors and organ motion uncertainties. For 60 breast cancer patients (24 resected with negative node involvement, 13 resected with positive node involvement and 23 ablated) who were treated with three different irradiation techniques, these uncertainties are simulated. The delivered dose distributions in the lung were recalculated taking positioning uncertainty and breathing effects into account. In this way the real dose distributions delivered to the patients are more closely determined. The positioning uncertainties in the anteroposterior (AP) and the craniocaudal (CC) directions are approximated by Gaussian distributions based on the fact that setup errors are random. Breathing is assumed to have a linear behavior because of the chest wall movement during expiration and inspiration. The combined frequency distribution of the positioning and breathing distributions is obtained by convolution. By integrating the convolved distribution over a number of intervals, the positions and the weights of the fields that simulate the original 'effective fields' are calculated. Opposed tangential fields are simulated by a set of 5 pairs of fields in the AP direction and 3 such sets in the CC direction. Opposed AP + PA fields are simulated by a set of 3 pairs of fields in the AP direction and 3 such sets in the CC direction. Single frontal fields are simulated by a set of 5 fields. In radiotherapy for breast cancer, the lung is often partly within the irradiated volume even though it is a sensitive organ at risk. The influence of the deviation in the dose delivered by the original and the adjusted treatment plans on the clinical outcome is estimated by using the relative seriality model and the biologically effective uniform dose concept. Radiation pneumonitis is used as the clinical endpoint for lung complications. The adjusted treatment plans show larger lung complication probabilities than the original plans. This means that the true expected complications are often underestimated in clinical practice. The lung density variation during breathing is calculated from the maximal change in average density during tidal breathing. The change in density in the lung due to breathing is shown to have almost no influence on the dose distribution in the lung. The proposed treatment-plan adjustments taking positioning uncertainty and breathing effects into account indicate significant deviations in the dose delivery and the predicted lung complications.

Received 14 November 2001
Accepted 30 May 2002

Breast cancer constitutes the most common site of cancer for women worldwide (proportion around 25%). A large proportion of breast cancer cases are treated by radiation therapy. Successful breast cancer treatment should provide a long, disease-free survival. In randomized trials, radiotherapy given after breast-conserving surgery (resection) or removal of the whole breast (radical mastectomy) has been shown significantly to reduce locoregional recurrence compared with surgery alone (1, 2). Radiation therapy after surgery is at present very commonly administered to decrease local relapse in the breast. The treatment is usually administered with a fractionation scheme of 5 days per week for 5 weeks at a daily dose of 2 Gy and a total dose of 50 Gy (3–5). Because of the proximity of lung to breast tissue, part of the lung is often within the irradiated volume, thus receiving a high dose. The objective of breast cancer radiotherapy is to minimize the relapse rate, simultaneously reducing the side effects so that the trade-off between benefits and complications from treatment is improved (6–9).

In radiation therapy of breast cancer there are three widely applied treatment techniques. Patients having undergone breast-conserving surgery are treated using two tangential opposed wedged fields that properly cover the breast tissue, in some cases with a non-divergent posterior beam edge to minimize the irradiated lung volume. Beam

 ISSN 0284-186X

angles for wedged parallel-opposed beams are optimized to reduce the irradiated lung volume. For patients with lymphatic node spread, a third frontal beam is added. Ablated patients are treated with two opposing photon fields for regional lymph node areas and with one electron field for chest wall and parasternal lymph node areas (2–5).

The clinical results of radiotherapy strongly depend on the ability of the quality control to identify potential sources of errors, which can be accounted for during treatment planning. Accuracy in patient positioning is a prerequisite to ensure agreement between the calculated and the delivered dose distribution to the patient but may well be one of the weakest parts of the radiotherapy process (10–13). Variations in dose distribution and in dose delivery can contribute to underdosage of the tumor or overdosage of normal tissue, which is potentially related to a reduction of local tumor control and an increase in side effects. Such variations in delivered dose distribution can be a consequence of patient setup inaccuracies. To identify localization errors in patient setup, portal films or electronic portal imaging devices have long been used for the verification of field alignment (14). Organ motion, and particularly breathing, is another source of treatment inaccuracy to be taken into account. Breathing motions can produce deviation of the delivered dose distribution compared to the calculated CT-based treatment plan and the effect in the dose-volume histograms (DVHs) can be significant (15–18). Breathing also affects the density of the lung, thus affecting the calculated dose (19, 20).

In this study, a method to model the effect of positioning and breathing uncertainties in breast cancer radiotherapy for the three treatment techniques is examined. The deviation between the calculated and the delivered dose distribution introduced by these uncertainties is estimated. This deviation is approximated by calculating the DVH of the lung from the original treatment plan and the one adjusted to the actual conditions. These changes in the dose distributions influence the predicted complication probabilities of the lung as well as the estimation of dose-response parameters.

MATERIAL AND METHODS

Patient selection

The study material comprised 60 consecutive patients treated with radiotherapy for breast cancer at Tampere University Hospital between 1996 and 1998. Thirty-seven patients had undergone breast-conserving surgery and 23 had had mastectomies. From the former group of patients, 24 had negative local lymph node involvement (R −) and were treated postoperatively with two, almost opposed, tangential photon beams and 13 patients had positive lymph node involvement (R +) and one additional frontal photon field was applied. Ablated patients (A) were treated with two opposite anterior–posterior photon fields for regional lymph node areas and with one electron field for chest wall and parasternal lymph node areas. The average volume of the irradiated lung from those treatment techniques was $1\,229 \pm 331$ cm^3 (median 1196 cm^3; range 448–1962 cm^3). Radiotherapy was started 4–8 weeks after surgery. The mean age of the patients was 58.5 ± 10.6 years (median 57.5 years; range 38–79 years).

Patient positioning and imaging

During CT acquisition, the patients were in supine position with both arms abducted from the body above the head. This position was maintained at the simulator and during the treatment, for all patients. The advantage of this position is the comfort that it affords the patients, since they can clasp their hands and therefore feel more relaxed. Furthermore, this symmetrical position makes it easier to match and reproduce adjacent fields between the different fractions of the treatment. CT slices were taken at intervals of 15 mm (R − and R +) or 20 mm (A) covering the whole assumed planning target volume (PTV) area and the whole lung volume. The pixel size in the CT image was about 1.3 mm and the slice thickness 8 mm.

Target definition and dose prescription

The issues of target volume localization, dose distribution inhomogeneities and radiation-induced complications both from tumor and lymph node irradiation are important in breast cancer radiotherapy. It is also important to define the aim of therapy (radical or palliative), since this influences the choice of the volume to be treated, the radiation dose, and the treatment technique. According to ICRU 50 recommendations (21, 22), PTV consists of the clinical target volume (CTV) and a margin to account for organ motion and setup errors. Some anatomical landmarks are usually included to help physicians delineate the PTV. In the treatment techniques studied, the CTV and PTV were defined and delineated according to the guidelines of the clinical protocol used for breast cancer treatment. The CTV consisted of the breast parenchyma (chest wall in the case of postmastectomy treatment) and the lymph nodes in the internal mammary chain, in the fossa, and in the axilla. A margin of 9–14 mm, depending on the directions of the setup errors and breathing, was added to the CTV, defining the PTV.

For node-negative patients, the CTV includes the entire breast, including the fatty tissue and skin, whereas for node-positive patients the thoracic wall, the ipsilateral internal mammary and axillary and supraclavicular lymph nodes are also included. More specifically, for node-negative patients, the PTV extends to the lowest point of the caput humeri and caudally to the inframammary fold. Medially, the PTV extends to the ipsilateral margin of the sternum and laterally to the lateral border of the breast. For node-positive patients, cranially, the PTV extends to

the cranial edge of the first rib at the costosternal junction and caudally to the inframammary fold. The medial border of the PTV is drawn 10 mm ipsilaterally of the midline of the sternum and, laterally, extends to the lateral border of the breast and axilla. For ablated patients, the chest wall and the regional lymph node areas (axillary, supraclavicular and parasternal) were included in the PTV.

The radiation dose was specified at the ICRU reference point (22). The prescribed total radiation dose was 50 Gy, given in 5 fractions per week at a daily dose of 2 Gy (Figs. 1–3, lower tables). There were some variations in dose prescription, owing to changes in practice in the clinic. The patients received 50 Gy from photon or electron irradiation, depending on the site and the case (3). The dose inhomogeneity within the target volume was usually within $\pm$ 5% of the prescribed dose.

Beam setup

One fraction of the patients with unilateral stages I and II invasive breast cancer was treated with segmental resection, axillary dissection and radiation. In these cases, the rate of local recurrence after conservative surgery for early breast cancer diminishes by using postoperative radiotherapy. The most common treatment techniques applied are the 3-field technique and the medial and lateral tangential 2-field techniques, which conform well to the PTV. To irradiate the breast (R $-$), the chest wall, and regional lymph nodes, two opposite tangential 5- or 6 MV photon wedge fields are used (Fig. 1, upper graph). The irradiation of lung tissue in the cranial-caudal direction is reduced by collimator rotation. Although a good distribution can often be achieved with a parallel-opposed pair of fields, it is sometimes necessary to alter the beam angles by a few degrees (6–8°) in order to avoid the underlying lung. In the middle graph of Fig. 1, a perspective view of the patient anatomy and field geometry can be seen. In this case the tissues of interest are the target volume (to be irradiated), the lung and the normal tissue stroma.

In the R $+$ case, in addition to the two tangential fields a frontal photon field was applied to irradiate the lymph nodes in the apex of the axilla and supraclavicular fossa (Fig. 2, upper graph). This anterior isocentric field was set up in the simulator and the dose distribution was calculated without PTV delineation in the treatment planning system. This treatment configuration is demonstrated more clearly in the middle graph of Fig. 2, where it is shown how the third field treats the local lymph nodes. In the tangential field treatment, a loss of function in a certain volume of lung usually has no clinical importance. It is estimated that when the distance from the deep margin of a tangential field to the inner part of the chest wall at the central axis of the field is 1.5 cm, approximately 6% of the ipsilateral lung volume is irradiated.

For the ablated patients, the treatment plan consists of two opposite photon fields for regional lymph node areas

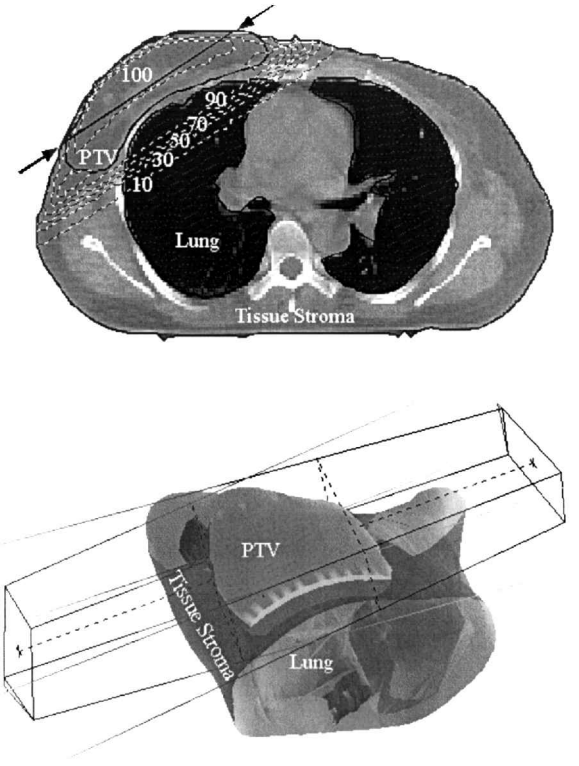

Physical Parameters	
Irradiation modality	Photons
Beam Energy	5 or 6 MV
Beam orientation	2 tangential fields angles: ~ 35° and 215°
Fractions	25
Prescribed dose	50 Gy
Clinical Parameters	
Internal Target Volume	entire breast (fatty tissue and skin)

Fig. 1. Upper graph: The reference CT slice of a resection—node-negative patient is shown. The anatomical structures involved in this clinical case are illustrated together with the applied beam configuration and the dose distribution delivered to the patient. *Middle graph*: Three-dimensional demonstration of the radiation treatment giving a better depiction of the beam setup and its geometrical relation to the irradiated site. In this way the effects of breathing and positioning uncertainties on the dose delivery can be better understood. *Lower table*: Quantitative summary of the physical and clinical parameters that characterize this clinical case and the applied radiation treatment.

(axillary, supraclavicular) and one electron field for chest wall and parasternal lymph node areas (Fig. 3, upper graph). The PTV was not delineated in the CT images. The outlines of the fields were defined directly on the conventional simulator film. The thickness of the chest wall was determined from the CT slices and converted to electron beam energy. Thereafter, the fields were set up in the treatment planning system. A descriptive view of this treatment configuration is shown in the middle graph of

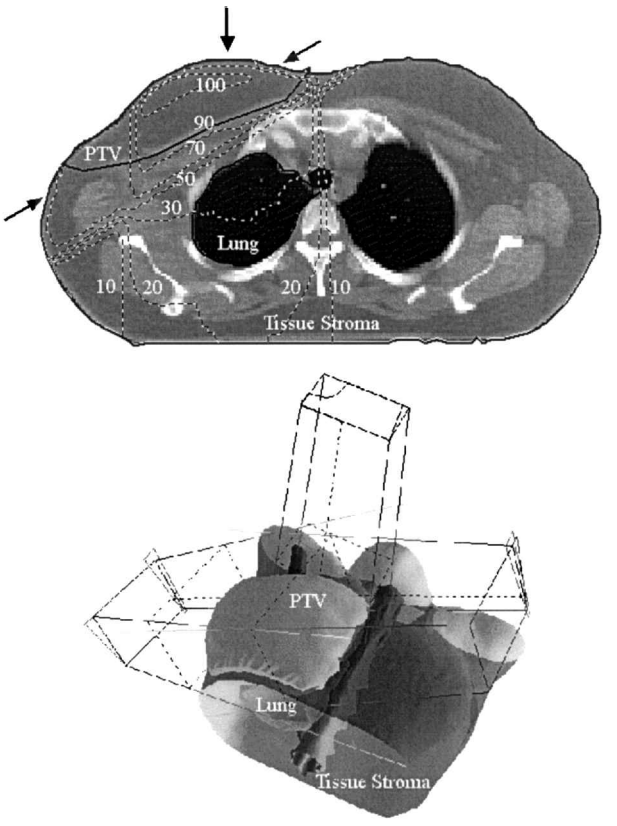

Physical Parameters	
Irradiation modality	Photons
Beam Energy	5 or 6 MV
Beam orientation	2 tangential fields angles: ~ 35° and 215° + 1 frontal field
Fractions	25
Prescribed dose	50 Gy
Clinical Parameters	
Internal Target Volume	entire breast (fatty tissue and skin) thoracic wall and lymph nodes (ipsilateral internal mammary and axillary, supra-clavicular)

Fig. 2. Upper graph: CT slice of a resection—node-positive patient is shown. The dose-limiting normal tissues (lung and normal tissue stroma) and the planning target volume (PTV) involved in this clinical case are illustrated together with the isodose map and the applied beam orientation. *Middle graph*: The applied treatment technique is demonstrated in space (3-dimensions) to depict the association of the beam configuration with the patient. *Lower table*: Quantitative description of the applied radiation treatment and the clinical parameters characterizing the case.

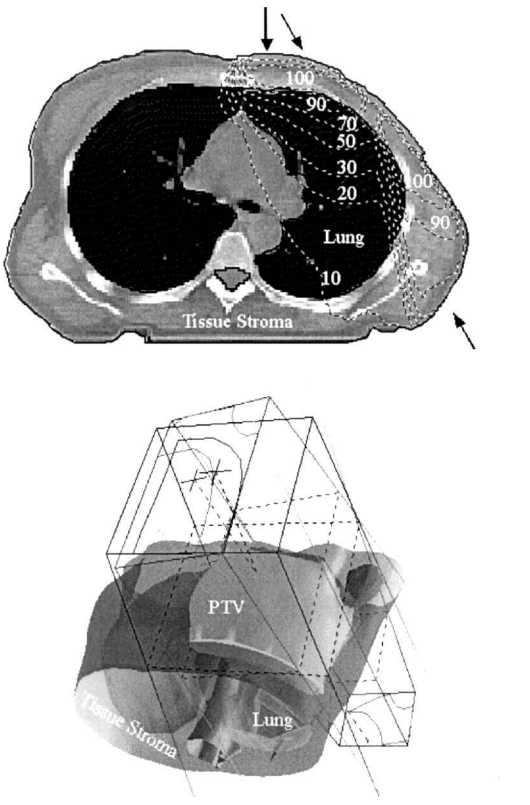

Physical Parameters		
Irradiation modality	Photons	Electrons
Beam Energy	6 and 25 MV	12 MeV
Beam orientation	2 anterior-posterior fields	1 frontal field
Fractions	25	25
Prescribed dose	50 Gy	50 Gy
Clinical Parameters		
Internal Target Volume	regional lymph nodes (axillary, supraclavicular)	chest wall, parasternal lymph nodes

Fig. 3. Upper graph: CT slice of an ablated (mastectomy) patient is shown. The anatomical structures of the lung and the normal tissue stroma involved in this clinical case are illustrated. The irradiating fields of the treatment and the isodose distribution are also shown. *Middle graph*: The geometrical relation of the beam setup with the breathing and positioning uncertainties is demonstrated by a 3-dimensional view of the applied treatment. *Lower table:* Quantitative summary of the physical and clinical parameters characterizing the radiation treatment applied. It is also shown that different regions of the planning target volume (PTV) are treated by different radiation modalities.

Fig. 3, where the blocked areas of the fields are also presented.

Dose calculation

The quality and accuracy of the delivered treatment strongly influence the clinical outcome. In this study, different sources of variation in treatment planning of breast cancer patients were estimated. The dose distribution was generally specified so that the minimum dose to PTV was 95% of the specified target absorbed dose. DVHs were calculated for the lung volume on the affected side. In the treatment planning process, different volumes were defined according to ICRU report 50. PTV delineation and dose calculation were carried out in a 3D treatment planning system (CADPLAN, Varian Associates Inc.).

Positioning uncertainty

Precisely to reproduce the patient position approximately

25 times during the course of a treatment is a challenging task requiring highly competent technologists with great concentration and experience. The geometry of the setup must be reproduced from simulation to treatment and during all the subsequent treatments. Otherwise, the delivered dose to the patient will differ from the planned dose, and consequently the treatment outcome may also be different from the expected one (23–25).

Model for calculating positioning uncertainty

Positioning uncertainty can be approximated by a Gaussian distribution. The Gaussian distribution is suitable in this case because it describes the distribution of random observations from many experiments. Furthermore, it appears adequately to describe the distribution of the parameter estimations of most probability distributions. Positioning uncertainty can be estimated in different directions (Fig. 4, anterior-posterior and cranial-caudal direction). Therefore, the following two equations were used to describe position variability:

$$f_{P,Y}(y) = \frac{1}{\sigma_y\sqrt{2\pi}} \exp\left(-\frac{(y-\bar{y})^2}{2\sigma_y^2}\right) \quad [1]$$

$$f_{P,Z}(z) = \frac{1}{\sigma_z\sqrt{2\pi}} \exp\left(-\frac{(z-\bar{z})^2}{2\sigma_z^2}\right) \quad [2]$$

where y and z are the positions in anteroposterior (AP) and craniocaudal (CC) directions in the beam coordinate system respectively. $\bar{y}$ and $\bar{z}$ are the mean values of the position and σ_y and σ_z are the standard deviations in the corresponding directions. The lateral positioning uncertainty was not accounted for in the study because of lack of an estimate of its magnitude from local measurements or from related literature. The systematic errors are considered to be zero, since no available clinical input for them was available.

In Table 1 a summary of the values for the positioning uncertainties determined in various studies for different directions is presented. The mean values of the reported standard deviations for the AP and CC directions were used in Equations [1] and [2], giving the Gaussian distributions shown in the upper diagrams of Fig. 4. The different bins of the histograms simulate the Gaussian distribution in each direction. The positions and the weights of these bins are calculated by integrating the Gaussian distribution over the following intervals ($-\infty$, -2.5; -2.5, $+2.5$; $+2.5$, $+\infty$) (in mm) for the AP direction and over the intervals ($-\infty$, -3.5; -3.5, $+3.5$; $+3.5$, $+\infty$) for the CC direction (Table 2). In the middle graph of Fig. 4, the combined distribution of the positioning uncertainties from the AP and CC directions is shown. This distribution can be simulated by a 3-dimensional histogram whose bins represent the different fields that could replace the fields of the original treatment plan in an attempt to simulate the clinical situation. In the lower diagram of Fig. 4, the positions and the heights of these histogram bins are represented by arrows that correspond to the positions and the weights of the simulating fields.

Breathing effects

In recent years there has been increased activity at various centers in measuring and reducing breathing-induced motion in radiotherapy. Breathing motions introduce inaccuracies in CT-based treatment plans. Sizeable errors in organ volume, position and shape can occur, which can significantly affect the calculation of the delivered dose distribution. These points are examined in a study where identical treatment plans performed on CT scans taken during quiet free breathing and during breath-hold at normal inspiration and expiration are compared (15, 18). Up to 14% variation in liver volume was observed, resulting in 40% variation in the calculated normal tissue complication probability (NTCP) (20). Consequently, the deviation between the calculated and the delivered dose distributions may have a significant effect on the treatment outcome. For the lung, an accurate description of the radiation dose received is even more complex because lung volume changes inherently, due to breathing. Breathing may also affect the calculation of the radiological path

Table 1

Positioning uncertainties involved in breast cancer treatment reported in the literature

Author	Standard deviation (SD)		Technique	SD determination
	AP (mm)	CC (mm)		
Mitine et al. (12)	3.0	5.8	Fixed SSD	SD all together
Gagliardi et al. (7)	2.9, 3.3	5.3	SAD	SE = $\sqrt{\text{pooled variance}}$
Creutzberg et al. (10)	4.6	–	SAD	SD all together
Fein et al. (26)	4.4, 3.2, 4.4	6.3	SAD	SD = $\sqrt{\text{pooled variance}}$
Pouliot & Lirette (14)	1.7	–	SAD	SD all together
Mean value	3.4	5.8		

Abbreviations: AP = anteroposterior direction; CC = craniocaudal direction; SD = standard deviation; SE = standard error.

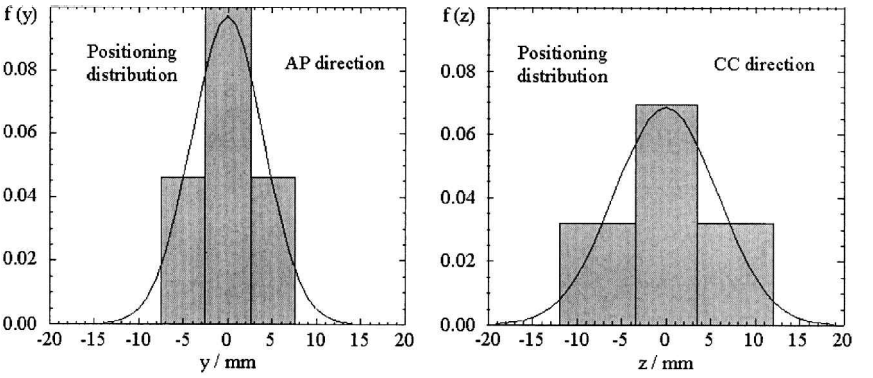

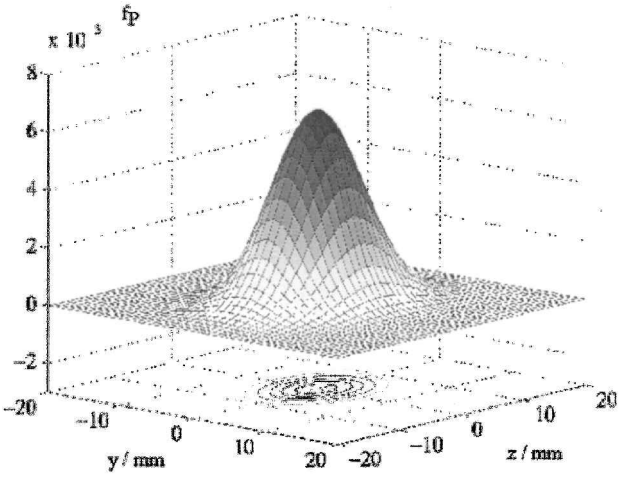

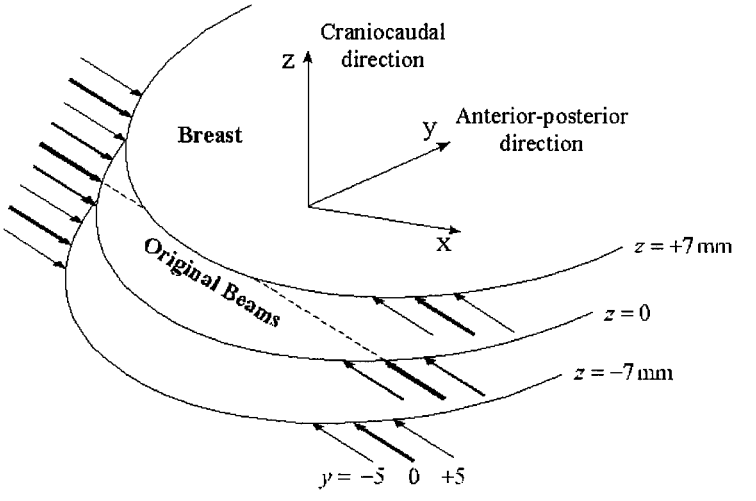

Fig. 4. Upper diagrams: The two diagrams demonstrate the error distribution of the patient setup in the y (anteroposterior (AP)) and z (craniocaudal (CC)) directions. The area below the two curves is normalized to the weight of the field (in this case it is assumed to be one). The theoretical (curve) distributions were simulated by histograms having the same integral area. The positions and the heights of the histogram bins represent the positions and the weights of the fields that will simulate the original 'effective field' in the corresponding direction. *Middle graph*: The joint 3-dimensional uncertainty distribution of patient setup. The volume under the surface was normalized to the weight of the simulated field. This surface is a combination of the curves shown in the upper diagrams and is simulated by a combination of the corresponding histograms. *Lower graph*: The true dose distribution in the patients is simulated by 9 pairs of fields (denoted as arrows) (3 pairs in every direction), which have different entrance points and weights, subjected to the specifications imposed by the simulation of the setup uncertainties.

Table 2

Field positions, weights and doses to calculate the true delivered dose. The correction was applied on the three treatment techniques according to their beam orientations

Field direction	Field shift (cm)	Weight/dose (Gy)	
	AP-direction		
	0	0.30	
	−0.6, 0.6	0.24	
Tangential	−1.2, 1.2	0.11	
	CC-direction		
	0	0.46	23.0
	−0.7, 0.7	0.27	13.5
	Total	1.00	50.0
	AP-direction: −0.5, 0.5	0.17	
	0	0.24	
Anteroposterior	CC-direction: −0.7, 0.7	0.21	
	Total	1.00	50.0

Abbreviations: AP = anteroposterior; CC = craniocaudal.

length to the tumor, thus affecting dose calculation and beam weighting. Path length changes of 1 cm or more in the thorax and abdomen have been reported, which could lead to changes of 2–3% in the tissue–phantom ratio for a 15 MV beam (20, 25).

Model for calculating breathing effects

The chest wall movement during breathing expiration and inspiration is shown in the upper left diagram of Fig. 5 (20). The simulating breathing motion is a simplification of the true breathing curve. However, the shape of the breathing cycle can change, depending on the kind of breathing performed (free-breathing, instructed periodic breathing, deep inspiration breath-hold, etc.). The point of exhalation is generally more reproducible than that of inhalation. Results have shown that when verbal breathing instructions (i.e. when to inhale and exhale) are given to patients for a period of time, this helps to improve the reproducibility in breathing (16). If the breathing is assumed to be linear, which is a good approximation of the true shape to a degree that is sufficient for our analysis, then the positional distribution of the anterior chest wall can take the shape shown in the upper left diagram of Fig. 5. Consequently, the following step function (shown in the upper right diagram of Fig. 5) can approximate the frequency distribution function due to breathing, f_B:

$$f_B(y-\bar{y}) = \begin{cases} \dfrac{1}{2a} & |y-\bar{y}| \le a \\ 0 & \text{otherwise} \end{cases} \quad [3]$$

a represents the chest wall displacement in the AP direction. In this work, a value of a equal to 1.0 cm (breathing amplitude of 0.5 cm) was used estimated by different studies (18–20). However, the breathing amplitude used for lateral tangential fields was smaller, depending on their angle in respect to the breathing direction.

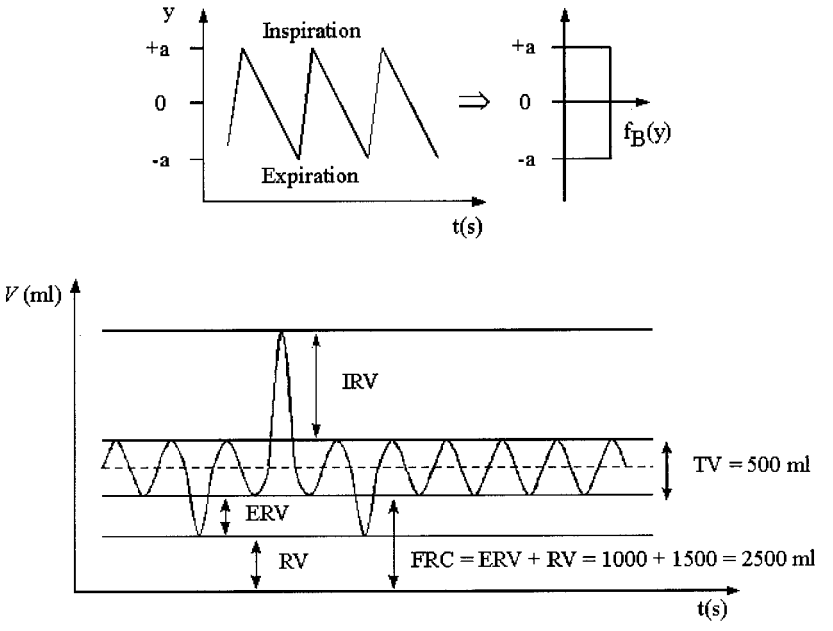

Fig. 5. Upper diagrams: The chest wall displacement as a function of time was derived from the literature. Assuming a linear displacement with time, the corresponding frequency distribution function is calculated (approximated by a step function) to be used for the estimation of the uncertainty caused by breathing. *Lower diagram*: The variation in gas volume in the lungs as a function of time is shown. The relationships between the different volumes of the lung participating in the breathing process are also presented. The range of the simultaneous change in lung density that takes place during breathing is subsequently estimated.

Lung density effect

The stretching and retraction that take place during respiration cause periodical changes in lung density. In particular, when the patient is lying on the treatment table, the lung density becomes inhomogeneous over both time and lung volume. Inclusion of a lung density correction factor may cause a reduction in the amount of wedge compensation needed in the irradiating fields (19, 20). Estimation of the variations in lung density during breathing can be made through the lung volume variations.

The air volume that is inhaled and exhaled in one breath is called Tidal Volume (TV). At rest, the TV is approximately 500 ml. After a tidal inhalation, a further 3000 ml air can be inhaled leading to the Inspiratory Residual Volume (IRV). Expiratory Reserve Volume (ERV) is the air volume (approximately 1000 ml) that can be further exhaled after an active effort. After extreme expiration, there will still be approximately 1500 ml of air left in the lungs, which is called the Residual Volume (RV). Functional residual capacity (FRC) is the sum of ERV and RV (cf. Fig. 5, lower diagram). The maximal deviation from the average density during tidal breathing can then be approximated by the following equalities:

$$\frac{\Delta_\rho}{\bar{\rho}} = \frac{\Delta V}{V} = \frac{\frac{1}{2}TV}{FRC + \frac{1}{2}TV} = \pm\frac{250\text{ ml}}{(2\,500 + 250)\text{ ml}}$$

$$= \pm 0.091(9.1\%)$$

where Δ_ρ is the change in density over one breath, $\bar{\rho}$ is the mean density of the lung, ΔV is half of the air volume in TV and $\bar{V}$ is the average air volume in the lungs. Using the values 500 and 2500 ml for TV and FRC, respectively, this formula gives a lung density variation $(\Delta_\rho/\bar{\rho})$ of $\pm 9.1\%$. To estimate the effect of this variation on the dose distribution, the mean CT number of the lung was changed by $\pm 9\%$ in each CT image, based on the fact that CT numbers are related to the density of the underlying anatomical structures.

Model combining positioning uncertainty and breathing effects

In order to estimate the combined effect of the breathing and positioning uncertainties, the overall uncertainty in the direction along the CT slices can be calculated as a convolution of the two distribution functions, providing they are assumed to be independent (17, 26). Here, it is assumed that the movement caused by breathing occurs only in the AP direction of the patient coordinate system. It is also assumed that the CT images represent the mid-tidal breathing phase.

The mean value of the setup standard deviation for the AP direction is used in Equation [1] to calculate the corresponding positioning frequency distribution function. By convolving this distribution function with the breathing frequency distribution function given by Equation [3], the combined frequency distribution $f_B(y) \otimes f_P(y)$ can be calculated.

$$f_B(y) \otimes f_P(y) = \int_{-\infty}^{\infty} f_B(\tau) \cdot f_P(y - \tau)\, d\tau \qquad [4]$$

The convolved distribution can be simulated by a 5-bin histogram through integrations over those 5 intervals shown in the upper left diagram of Fig. 6. The integral area below the curve of the distribution should be normalized to the weight of the fields used in the original treatment plan. The positions and the weights of the histogram bins were calculated by integration of the convolution distribution over the following intervals $(-\infty, -9.0)$, $(-9.0, -3.0)$, $(-3.0, 3.0)$, $(3.0, 9.0)$ and $(9.0, \infty)$ (in mm). The frequency distribution function in the CC direction consists of the positioning uncertainty part only and its simulation is shown in the upper right diagram of Fig. 6. In the lower left graph of Fig. 6, the combined distribution of the convolved positioning and breathing uncertainties for the AP direction and of the positioning uncertainty for the CC direction is shown. This distribution is again simulated by a 3-dimensional histogram that attempts to reproduce the actual treatment situation. The positions and weights of the simulating fields corresponding to this histogram are shown in the lower right diagram of Fig. 6.

Adjusted treatment plan calculation

For the three different techniques applied in this study, the correction of each beam was done according to its direction against the patient. The original treatment plan of the R− case consists of two tangential fields. In the AP direction, the movements of the patient against these fields were simulated in the adjusted plan by 5 pairs of fields. Three such sets of fields were used to simulate the uncertainty distribution in the CC direction. The original treatment plan of the R+ case includes one additional frontal field, whereas the original plan of the mastectomy case consists of three fields oriented in the AP direction. In the A case, the original photon fields were simulated by 3 pairs of fields in the AP direction and three such sets of fields in the CC direction. For the frontal photon and electron fields of the R+ and A cases respectively, the uncertainty adjustment was made by using a set of five fields covering both the AP and CC direction. That is, because the breathing effects in the lateral directions are neglibile.

The field positions and weights applied during the positioning adjustment part are presented in Table 2. The uncertainty distribution of the original tangential fields is simulated in the AP direction by adding new sets of fields but with different y values (y: 0.0, ± 0.6, ± 1.2 cm) and different respective weights (0.30, 0.24, 0.11). In the CC direction, the new z values of the fields are (z: 0.0, ± 0.7 cm) with respective weights (0.46, 0.27) (cf. Fig. 6, upper diagrams). The original fields that are oriented anteropos-

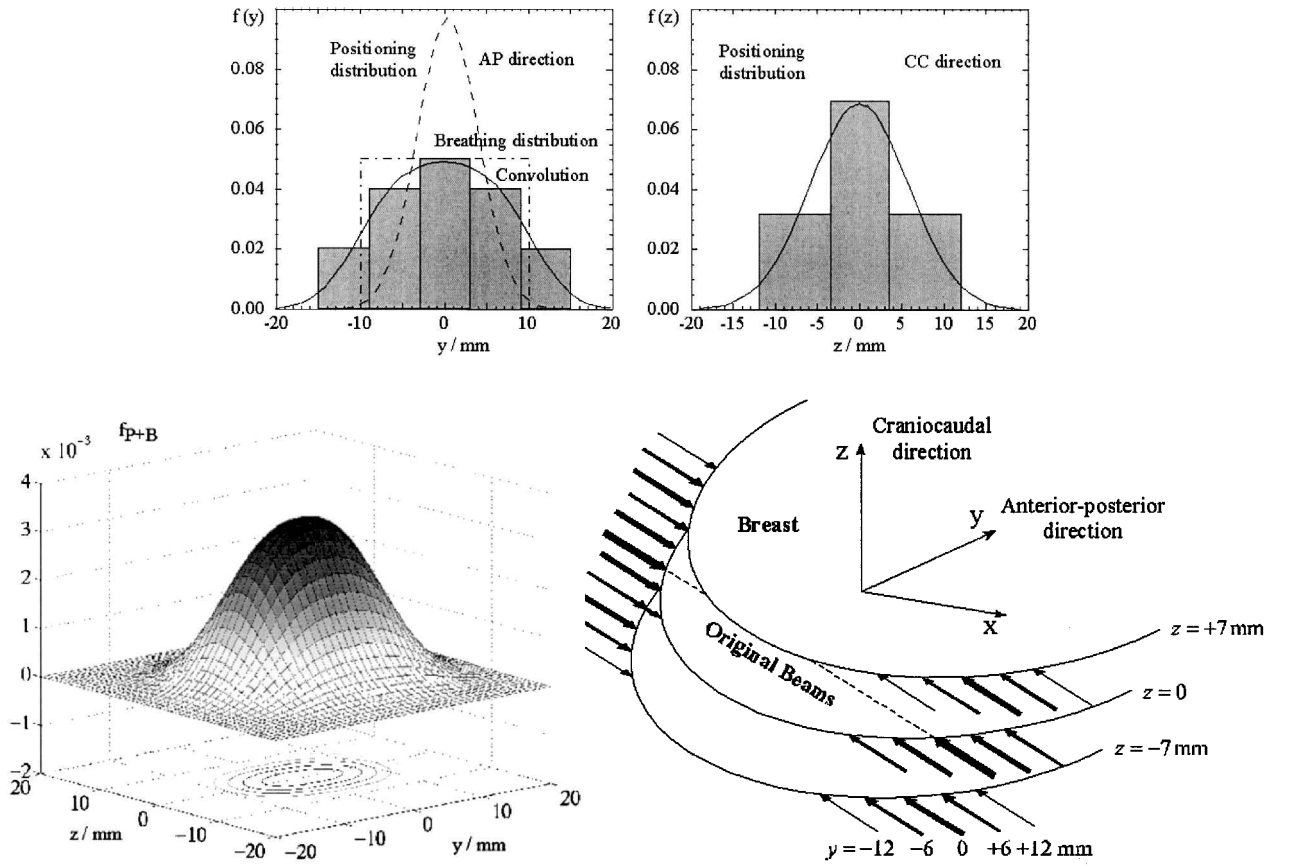

Fig. 6. Upper diagrams: The two diagrams demonstrate the error distribution of the patient setup in the y (anteroposterior (AP)) and z (craniocaudal (CC)) directions. The distribution in the AP direction is the result of a convolution of the patient positioning and breathing uncertainties. The area below the two curves is normalized to the weight of the simulated field (in this case it is one). The theoretical distributions (curves) are simulated by step histograms having the same integral area. The positions and the heights of the histogram bins represent the positions and the weights of the fields that will simulate the original 'effective field' in the corresponding direction. *Lower left graph*: The joint 3-dimensional uncertainty distribution imposed by patient setup errors and breathing effects. The volume under the surface was normalized to the weight of the simulated field. This surface is a combination of the curves shown in the upper diagrams and is simulated by a combination of the corresponding histograms. *Lower right graph*: The true dose distribution in the patients is simulated by 15 pairs of fields (a set of 5 pairs in the AP direction and 3 such sets in the CC direction), which have different entrance points and weights, subjected to the specifications imposed by the simulation of the combined setup and breathing uncertainties.

teriorly (R +, frontal field and A electron field) are simulated by sets of five fields with position values (0.0, y: ± 0.5, z: ± 0.7) and respective weights (0.24, 0.17, 0.21) (cf. Fig. 4, upper diagrams). Using the new treatment configurations for the three clinical cases and the prescribed doses given in Table 2, the adjusted DVH could be calculated for each case. In conclusion, the adjusted treatment plans had to use up to 30 fields to model the positioning uncertainty and breathing effects on the dose distribution.

The relative seriality model

The radiobiological model that has been used throughout this work for describing the dose-response relation of the lung is the linear-quadratic Poisson model (27–29).

$$P(D) = \exp(-e^{e\gamma - (D/D_{50})\cdot(e\gamma - \ln\ln 2)}) = \exp(-e^{e\gamma - \alpha nd - \beta nd^2}) \quad [5]$$

where $P(D)$ indicates the probability of inducing a certain injury to the lung (radiation pneumonitis in this case) when it is irradiated uniformly with a dose D, $d = D/n$ is the dose per fraction and n is the number of fractions applied. D_{50} is the dose which gives a response probability of 50% and γ is the maximum normalized value of the dose-response gradient. The linear-quadratic model also accounts for the fractionation scheme applied; α and β are the fractionation parameters of the model and account for the expected early and late effects. Parameters D_{50} and γ (or α and β) are specific for every organ and specific for the kind of injury (endpoint) considered and can only be derived from clinical data.

Each lung dose distribution was corrected using the linear-quadratic model to a 2 Gy per fraction schedule. Thus, each dose step in the histograms was corrected separately. The α/β value assumed in the fractionation correction was 3 Gy. The radiation sensitivity was

assumed to be homogeneous throughout the lung volume.

Both D_{50} and γ depend on the initial number of functional subunits (FSUs) in the lung. The complications observed in normal tissues following the therapeutic use of radiation have been described in terms of inactivation of FSUs (30). The organization of the FSUs is described in terms of serial, parallel or, more generally, a combination of these two structures. Many researchers have provided expressions for estimating the probability of complications using models that account for the volume effect, which stems from the FSU infrastructure of the organs. The volume effect describes how the tolerance dose increases with decreasing partial irradiated volume of normal tissues. Organs with a serial infrastructure have a small volume dependence since every subunit is vital for organ function. For organs with a parallel infrastructure, a strong volume dependence can be expected since the organ can maintain most of its function even when a large proportion of its subunits is damaged.

In this work, the concept of the volume effect is treated by the model of relative seriality. For a heterogeneous dose distribution, the response of normal tissues is given by the expression (7, 8, 31):

$$P(\vec{D}) = \left[1 - \prod_{i=1}^{M} \left[1 - P(D_i)^s \right]^{\Delta v_i} \right]^{1/s} \quad [6]$$

where Δv_i ($= \Delta V_i / V_{\text{ref}}$) is the fractional subvolume of an organ that is irradiated compared to the reference volume for which the values of D_{50} and γ were calculated. $P(D_i)$ is the probability of response of an organ having the reference volume and being irradiated to dose D_i, as described by Equation [5], M is the total number of voxels or subvolumes in the organ and s is the relative seriality parameter that characterizes the internal organization of the organ. A relative seriality close to zero ($s \approx 0$) corresponds to a completely parallel structure, which becomes non-functional when all its functional subunits are damaged, whereas $s \approx 1$ corresponds to a completely serial structure which becomes non-functional when at least one functional subunit is damaged.

Usually, the whole volume of a healthy organ is used as the reference volume because the volume of an organ is related to the functional needs of the individual human being (32). In this clinical case, the whole lung constitutes the reference volume to which the model parameters D_{50} and γ refer (Table 3).

Radiobiological aspects of lung

Whenever radiotherapy is given with curative intent, there is a risk of serious damage to normal tissues, which increases with dose. Radiation effects on normal tissues are usually divided into two categories: early and late reactions (33).

Lung is an intermediate-to-late responding tissue, for which at least two separate radiation-induced effects (endpoints) are recognized: acute pneumonitis occurring 2–6 months after treatment, and fibrosis, which develops slowly over a period of several months to years (34). Lung is among the most sensitive of the late-responding organs, but because of the structural organization of its functional subunits, it only becomes dose limiting when large volumes of the lung are irradiated. For the endpoint of lung pneumonitis the α/β ratio is 2–4 Gy (34). Radiation injury of lung tissue is dependent on the total dose, the fractionation scheme, the irradiated lung volume and on the radiosensitivity of the individual patient.

The effect of radiation on the lung is a matter of great concern in breast irradiation. The volume of lung tissue included in the tangential fields should be kept to a minimum. However, in order to irradiate the chest wall, the inclusion of some lung volume is unavoidable. The prescribed target dose that is used in breast cancer is higher than the tolerance dose of the lung tissue. Consequently, damage to some lung tissue has to be accepted.

The biologically effective uniform dose, $\bar{\bar{D}}$

The biologically effective uniform dose is the uniform dose that causes exactly the same tumor control or normal tissue complication probability as the real dose distribution (35, 36).

$$\bar{\bar{D}} = D_{50} \frac{e\gamma - \ln(-\ln(P(\vec{D})))}{e\gamma - \ln(\ln(2))} \quad [7]$$

For each patient, this concept finds the uniform dose that is biologically as effective as the dose distribution $D(\vec{r})$ delivered to the lung. For each patient, the effectiveness of the dose distribution applied is calculated by the relative seriality model and the set of parameters that describe the dose-response relation of radiation pneumonitis. The

Table 3

Dose-response parameters of lung (9)

Radiobiological parameters	Value	Reference Volume	Clinical endpoint
D_{50} (Gy)	26.0	Whole lung	Radiation pneumonitis
γ	2.0		
s (relative seriality)	0.031		

reason for using the concept of the biologically effective uniform dose is that each patient in the study population receives a different dose distribution. To be able to compare the dose distributions from the original and adjusted treatment plans in radiobiological terms, a concept such as $\bar{D}$ needs to be used. In this way, we can calculate how much higher is the dose that is effectively delivered to the lung.

RESULTS

In order to determine how the dose distribution at the edge of the fields is affected by the positioning and breathing uncertainties, dose profiles from the surface of the breast towards the central part of the lung were calculated for both the original and the adjusted treatment plans. The line along which the dose profile was calculated is shown in the upper diagram of Fig. 7.

For the R − case, the dose profile is perpendicular in direction to the axis of the tangential beams. This is plotted in the same diagram both for the original and the adjusted treatment plans (normalized to the ICRU report 50 reference point) to make a clearer comparison between them and to observe their differences (cf. Fig. 7, middle diagram). The curve is almost the same at the beginning (at the edge to the breast). The dip that is observed comes from the chest wall, which has a different density and structure from the breast tissue. It is apparent that inside the lung the dose gradient is smaller for the adjusted compared to the original treatment plan. The 80/20 penumbra for the adjusted plan is 15.3 mm, whereas for the original plan it is 9.5 mm.

For the ablation case (mastectomized patients), the dose profile has the same direction as the photon and electron beams simulating in practice a depth-dose curve (cf. Fig. 7, lower diagram). It is observed that the change in the dose profile inside the lung for the photon field is similar to the change noticed for the tangential fields (smaller dose gradient for the adjusted plan). For the electron field, it is shown that although the dose gradient is almost the same in the original and the adjusted plans, the integral dose in the latter plan is smaller.

The DVHs of the involved lung were computed for all the patients included in the study. The original plans are compared with the adjusted ones for the different treatment configurations. The mean cumulative DVHs (original and adjusted) for the three groups of patients (R −, R + and A) are presented in Fig. 8. Moreover, the corresponding mean cumulative DVHs of the PTV were calculated for the R − case. The difference in the corresponding histograms illustrates the average changes in the delivered dose distribution imposed by the positioning uncertainties and the breathing effects.

In the R − case (Fig. 8, upper left diagram), the gradient of the adjusted plan is lower than that of the original one. This is because the 'effective fields' are smeared out, being subjected to positioning and breathing uncertainties.

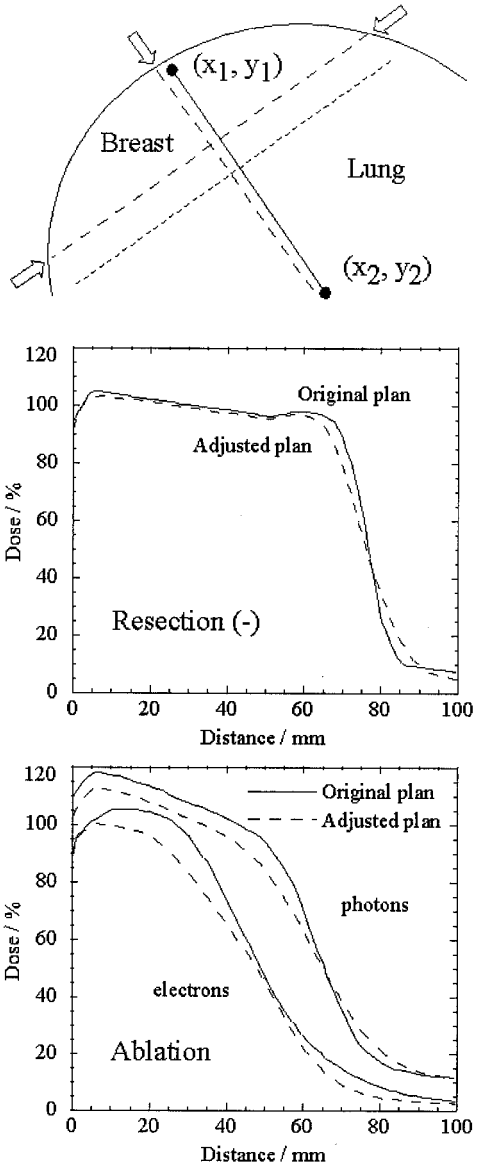

Fig. 7. A dose profile was calculated for the original and the adjusted treatment plans of a resected and an ablated patient. *Upper diagram*: The beams applied on the resected patient are tangential, though the dose profile is directed from the surface of the breast toward the center of the lung. In the case of the ablated patient, the direction of the beams almost coincides with that of the dose profile. *Middle diagram*: The first part of the curves (until the dip) is the dose inside the breast and the rest is the dose in the lung. It is illustrated that in the adjusted treatment plan the dose profile is smoother, with the dose changing less abruptly compared to the original plan. *Lower diagram*: The characteristics shown in the case of the resected patient are also present here for the photon field. The dose change is smoother for the adjusted treatment plan in the region of the lung. However, for the electron field, the dose profile of the adjusted plan is not smoother than the original plan but lower. This is because the contribution of the electron beam is distributed to a larger volume of the lung.

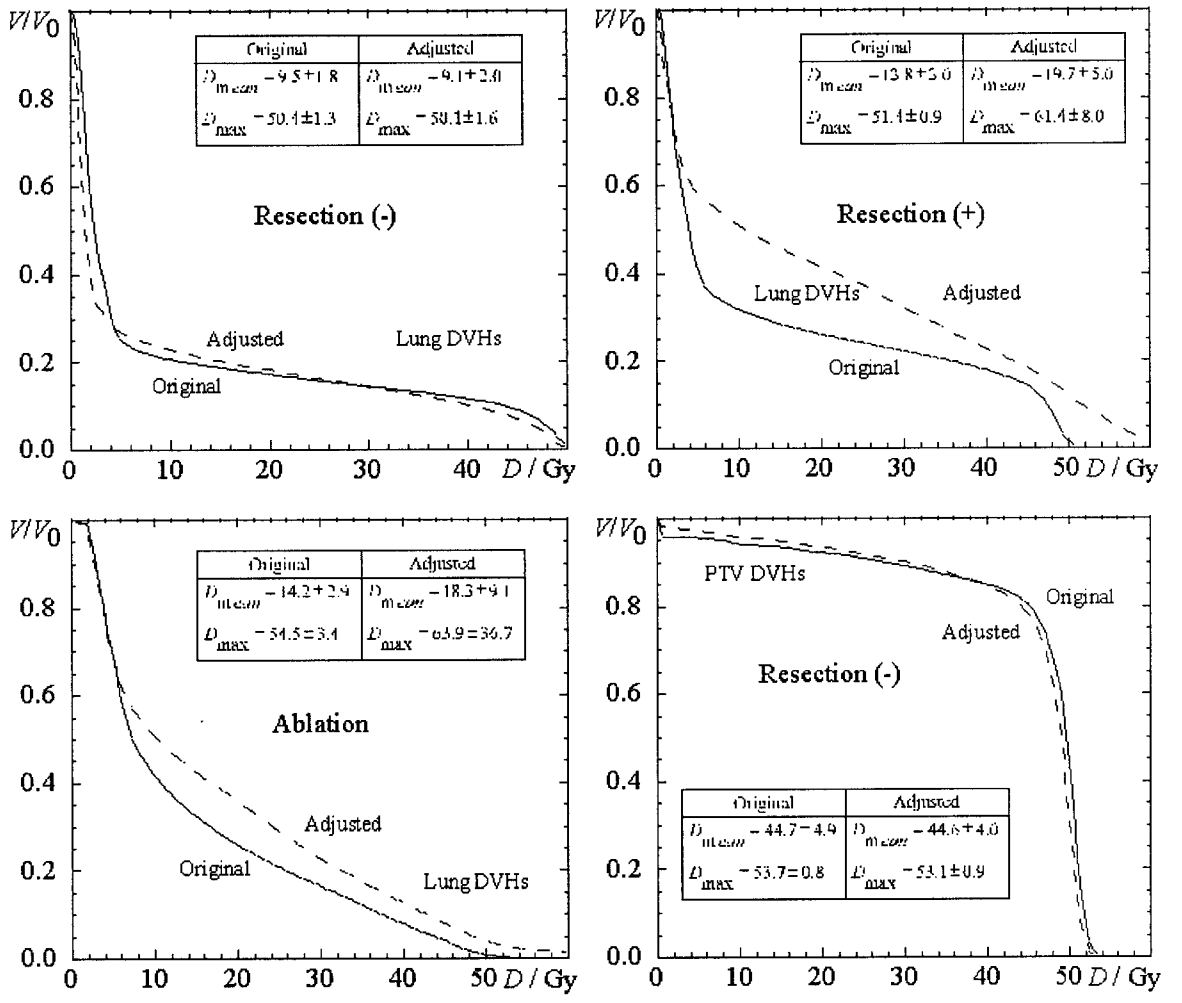

Fig. 8. Upper left diagram: The mean cumulative dose-volume histograms (DVHs) of the original and the adjusted treatment plans for the R − case were calculated. It is shown that the adjusted dose plans deliver low doses to a larger part of the lung and high doses to a smaller lung volume than the original dose plans. The mean and maximum doses of the two plans are also presented. *Upper right diagram*: For the R + case, it is shown that the mean cumulative DVH of the adjusted treatment plan is significantly higher than that of the original plan. This is also depicted by the mean and maximum doses of the two plans. *Lower left diagram*: The mean cumulative lung DVHs of the original and the adjusted treatment plans for the ablation (mastectomy) case are shown. Notice that the adjusted plan delivers a higher dose to the lung than the original plan, which is also demonstrated by the difference in their mean and maximum doses. *Lower right diagram*: The mean cumulative DVHs of the PTV (planning target volume) for the R − case show that the difference between the adjusted and the original treatment plans is small.

In the adjusted plan, a larger volume receives a lower dose than in the original plan. More quantitatively, this means that a larger volume will receive a dose between approximately 5 and 15 Gy in the adjusted plan. In both plans almost the same lung volume receives about 15–35 Gy. Finally, a larger volume in the original plan will receive a higher dose than the adjusted one. This is because the two treatment plans deliver almost the same integral dose, which means that if one plan delivers a higher dose over a volume of the lung, then it has to give a lower dose to another volume, as counterpart. This is also shown by the values of the average and maximum doses of the two histograms.

In the R + case (Fig. 8, upper right diagram), it can be seen that the dose delivered to the lung from the adjusted treatment plan is much larger than that from the original plan. Quantitatively, this difference is expressed by the corresponding mean and maximum doses (19.7 vs. 13.8 Gy and 61.4 vs. 51.4), respectively. In the ablation case (Fig. 8, lower left diagram), as in R +, the results show the lung receiving a much higher dose from the adjusted plan than from the original plan. A quantitative comparison of the two histograms shows that the mean and maximum doses from the former plan (18.3 and 63.9) are larger than the corresponding doses (14.2, 54.5) from the latter plan.

The effect of the lung density change due to breathing on the dose distribution was evaluated by changing the density of the lung in two selected patients. The two patients were chosen on the grounds of their irradiated lung volume at 20 Gy, which is almost the median of the histograms. For the patient with the small, irradiated volume (40 cm^3) the mean lung density was 0.261 g cm^{-3} (range 0.200 to 0.335 g cm^{-3}), whereas for the patient with the large irradiated volume (370 cm^3) the mean lung density was 0.200 g cm^{-3} (range 0.186 to 0.224 g cm^{-3}). The average lung density was changed by $+9\%$ in the end expiratory phase and -9% in the end inspiratory phase in each CT image. After recalculating the dose distributions for these cases, new DVHs were generated. Almost no difference was inferred by the adjustment of the lung density in the calculations. More specifically, the dose in the density-adjusted plan is approximately 0.5% higher than that in the original plan. This difference was not accounted for in the calculations on the influence of positioning and breathing uncertainties.

The expected lung complication probabilities were estimated by using the relative seriality model and a set of published radiobiological parameters that are compatible with this patient material (Table 3). For the three treatment techniques, the dosimetric information from the original and the adjusted DVHs was used. The results of these comparisons are summarized in Table 4. In all three cases, the calculated lung response probability P_I was larger for the adjusted plans than for the original plans. The difference is minor for the R− case but highly significant for the R+ and the ablation cases. This means that a significant underestimation of the expected complications was made during the radiobiological evaluation of the treatment plans.

Calculating the values of $\bar{D}$ for the different cases, it is shown that the effective dose difference in the R− case is only 0.4 Gy, whereas in the R+ and the ablation cases it is 4.32 and 3.58 Gy, respectively. Calculation of the relative complication probabilities shows that the risk of complications is actually 1.2 times higher for the R− case, 8.44 for the R+ and 10.56 for the ablation cases.

DISCUSSION

Quality control is of outmost importance in radiation therapy because of the existence of many potential sources of errors. Such errors, which take place during the delivery of the treatment to the patient, result in the degradation of the curative power and effectiveness of the treatment (37). Positioning uncertainties and breathing effects are the sources of such errors because they lead to a dose delivery that is different from the one originally intended (38, 39). The lung is usually the main organ at risk in radiotherapy for breast cancer, which is usually applied after conservative surgery or radical mastectomy. Therefore, restricting the dose to the lung to a minimum is one of the guidelines followed by clinically applied treatments.

However, deviation of the delivered from the planned dose distribution to the lung due to positioning and breathing uncertainties can be significantly large. Positioning uncertainties are greater in the CC direction than in the AP direction. These uncertainties were approximated by Gaussian distributions based on the fact that the setup errors are random. On the other hand, breathing is periodic (like a saw-toothed distribution) and its frequency distribution, which assumes that inspiration and expiration have the same length, was described by a step function. The effects of both sources of errors were simulated using realistic values and methods. However, the results of the dose-distribution adjustments are closely related to the treatment techniques examined and they are not applicable to other treatment configurations. For the R− case, the DVHs of the original and the adjusted treatment plans do not differ greatly, partly because their integral doses are almost the same (Fig. 8, upper left diagram). In this case, the displacement of the beams in respect of the lung results in only a small volume of the lung always lying in the high-dose region and a large volume lying in the intermediate-dose region. In the R+ and ablation cases, the dose of the adjusted DVHs is much higher than that of the original DVHs because the contribution of both the frontal supraclavicular photon and electron fields respectively becomes larger, leading to a significant increase in the

Table 4

Results of the dose distribution adjustment. Complication probabilities were calculated using the relative seriality model

Dose plans		Resection negative nodes	Resection positive nodes	Mastectomy
Original	P_{lung} (%)	0.010	2.65	1.17
	$\bar{D}$ (Gy)	14.41	18.58	17.67
Adjusted	P_{lung} (%)	0.022	25.02	13.53
	$\bar{D}$ (Gy)	14.81	22.90	21.25
Difference	Absolute P_{lung} (%)	0.012	22.37	12.36
	Absolute $\bar{D}$ (Gy)	0.40	4.32	3.58
	Relative P_{lung} (%)	1.20	8.44	10.56

integral dose to the lung (Fig. 8, upper right and lower left diagrams).

In the lower right diagram of Fig. 8, it is shown that the positioning and breathing uncertainties do not greatly affect the dose distribution to the PTV (calculated for the R − case). This is because the uncertainties studied have more influence on the tissues lying at the edges of the irradiating fields. Furthermore, the CTV, which is in the interior part of the PTV, seems to be completely irradiated with the planned prescribed dose (40).

The treatment planning system that was used in this work has a limitation concerning the maximum number of fields that can be used in a treatment plan. This technical problem restricted the simulation process from using a larger number of fields, approximating even more the frequency distribution functions of the different error sources (Figs. 4 and 6, upper diagrams). This means that the adjusted dose distributions, which were calculated in this work, are not the true delivered dose distributions but a reasonably good approximation of them.

The values of the positioning uncertainties and the breathing displacement used in this work were taken from the literature. However, the most appropriate way to carry out this study would be to estimate these uncertainty values from the same patient material using portal imaging or other treatment verification means. This information was not available for calculating the exact values. However, the clinicians consider the values that were used as a good approximation of the applied clinical practice.

The radiobiological parameter values applied to a certain patient material should be compatible with it. These parameters are derived from patient materials where the dose delivered to each patient and the follow-up records are available. Because the treatment methodologies among different institutions are likely to differ to some extent and the clinical information is still limited (imaging at a cellular level, accurate determination of the dose delivered to the patient, radiosensitivity of the individual patient, etc.), the derived parameters from such studies are subjected to these factors. In this study, the parameters taken from the literature have been derived without being adjusted for positioning uncertainties and breathing effects. On examining the treatment methodology applied for the derivation of the parameters and the study material, the compatibility of the parameters for evaluating the lung complications of the original plans was approved. For the adjusted plans, another set of parameters should have been used (derived from a patient material where positioning uncertainties and breathing effects have been taken into account). Such parameters have not been published in the literature, although there is a general belief that they should not differ significantly from those that have already been published. In any case, the purpose of this paper is not to make a precise quantification of the probability of change when positioning uncertainties and breathing are taken into consideration but to estimate the order of difference in the delivered dose in terms of treatment outcome. The ongoing recording of the follow-up results of the extended breast cancer material of the clinic will allow the derivation of relevant radiobiological parameters and verification of the results presented.

The influence of the density changes of the lung was also investigated. It was shown that the size of the change in the dose distribution was approximately 0.5%. This value was calculated by changing the CT numbers of the regions corresponding to the lung in the planning CT images. This process was based on the fact that the magnitude of CT numbers is related to the density of the underlying anatomical structure. In practice, the dose delivered to an organ is quantified by isodose charts or DVHs. This is an accurate description when the density of the organ is homogeneously distributed throughout its volume. However, when the organ is heterogeneous in density (like the lung) the appropriate way to quantify its volumetric dose distribution is by calculating its dose-mass histogram (DMH). This can be done by using the density map that is provided by the CT numbers of the planning CTs and the volume information from the treatment planning system. It is also more appropriate to use DMHs in calculations of the expected complication probability of lung, because density is related to the number of FSUs, which are responsible for the expression of a certain clinical endpoint (such as radiation pneumonitis).

For resected patients with negative or positive lymph node involvement or ablated patients treated with other beam configurations, a similar study should be carried out to estimate the influence of the positioning uncertainties and breathing effects on the delivered dose distribution, because this depends on the geometrical relationship of the treatment fields and the patient.

CONCLUSIONS

The combined effects of positioning uncertainties and breathing motions can introduce a significant deviation between the planned and the delivered dose distribution to the lung in breast cancer radiotherapy. One way to account for these effects is either to use a gated treatment technique, which usually means access to more sophisticated technology, or to simulate the true dose delivery by using a number of fields of different weights and entry points during treatment planning.

The density changes in the lung do not introduce significant alterations in the effectiveness of the delivered dose distribution. This inaccuracy in the delivered dose to the patient may lead to a significant underestimation of the expected probabilities of developing radiation-induced pneumonitis. A more detailed analysis of the consequences of positioning uncertainty and breathing effects on different treatment techniques, clinical structures, and cancer sites can be made using a more extensive patient material, since these effects stem from the dynamic geometrical relation of the beam configuration against the body or the irradiated site.

ACKNOWLEDGEMENTS

This work was supported mainly by grants from Cancerföreningen i Stockholm, Konung Gustav V:s Jubileumfond, the Research Center for Radiation Therapy and the Center of Excellence of the Swedish National Board for Industrial and Technical Development.

REFERENCES

1. Radiotherapy for cancer. Acta Oncol 1996; 35 (Suppl 7).
2. Bonadonna G, Hortobagyi GN, Gianni AM. Textbook of breast cancer. UK: Martin Dunitz, 1997.
3. Holli K, Pitkänen M. Tangential breast irradiation with or without internal mammary chain irradiation: results of a randomized trial. Radiother Oncol 1995; 36: 172–6.
4. Rajala J, Järvenpää R, Lahtela S-L, Holli K, Ojala A, Pikänen M. Lung reactions after postoperative radiotherapy of breast cancer; correlation of reaction grade to dose-volume histograms. Nordic Symp Radiat Oncol Tampere, 1999.
5. Pitkänen MA, Holli KA, Ojala AT, Laippala P. Quality assurance in radiotherapy of breast cancer. Variability in planning target volume delineation. Acta Oncol 2001; 40: 50–5.
6. Emami B, Lyman J, Brown A, et al. Tolerance of normal tissue to therapeutic irradiation. Int J Radiat Oncol Biol Phys 1991; 21: 109–22.
7. Gagliardi G, Lax I, Rutqvist LE. Radiation therapy of stage I breast cancer: analysis of treatment technique accuracy using three-dimensional treatment planning tools. Radiother Oncol 1992; 24: 94–101.
8. Ågren A-K, Källman P, Brahme A. Determination of the relative seriality of a tissue from its response to non-uniform dose delivery. In: Baltas D, ed. Modelling in clinical radiobiology. Germany: Albert Ludwig's University Freiburg, 1997: 127–41.
9. Mah K, van Dyk J, Keane T, Poon PY. Acute radiation-induced pulmonary damage. A clinical study on the response to fractionated radiation therapy. Int J Radiat Oncol Biol Phys 1987; 13: 179–88.
10. Creutzberg CL, Althof VGM, Huizenga H, Visser AG, Levendag PC. Quality assurance using portal imaging: the accuracy of patient positioning in irradiation of breast cancer. Int J Radiat Oncol Biol Phys 1993; 25: 529–39.
11. Lind BK, Källman P, Sundelin B, Brahme A. Optimal radiation beam profiles considering uncertainties in beam patient alignment. Acta Oncol 1993; 32: 331–42.
12. Mitine C, Dutreix A, van der Schueren E. Tangential breast irradiation: influence of technique of set-up on transfer errors and reproducibility. Radiother Oncol 1991; 22: 308–10.
13. Bel A, van Herk M, Bartelink H, Lebesque JV. A verification procedure to improve patient set-up accuracy using portal images. Radiother Oncol 1993; 29: 253–60.
14. Pouliot J, Lirette A. Verification and correction of setup deviations in tangential breast irradiation using EPID: gain versus workload. Med Phys 1996; 23: 1393–8.
15. Mah D, Hanley J, Rosenzweig K, et al. The deep inspiration breath-hold technique for the treatment of lung cancer: the first 200 treatments. Int J Radiat Oncol Biol Phys 1999; 45: 205.
16. Kubo HD, Hill BC. Respiration gated radiotherapy treatment: a technical study. Phys Med Biol 1996; 41: 83–91.
17. Lujan AE, Larsen EW, Balter JM, Ten Haken RK. A method for incorporating organ motion due to breathing into 3D dose calculations. Med Phys 1999; 26: 715–20.
18. Balter JM, Ten Haken RK, Lawrence TS, Lam KL, Robertson JM. Uncertainties in CT-based radiation therapy treatment planning associated with patient breathing. Int J Radiat Oncol Biol Phys 1996; 36: 167–74.
19. Hanley J, Debois MM, Mah D, et al. Deep inspiration breath-hold technique for lung tumors: the potential value of target immobilization and reduced lung density in dose escalation. Int J Radiat Oncol Biol Phys 1999; 45: 603–11.
20. Mageras G. Respiratory motion-induced treatment uncertainties. In: Kappas C, del Guerra A, Kolitsi Z, Damilakis Y, Theodorou K, eds. Medical physics. Bologna: Monduzzi Editore, 1999: 33–8.
21. Aaltonen P, Brahme A, Lax I, et al. Specification of dose delivery in radiation therapy. Recommendations by the Nordic Association of Clinical Physics (NACP). Acta Oncol 1997; 10 (Suppl): 1–32.
22. ICRU. Prescribing, recording, and reporting photon beam therapy. ICRU Report 50. Washington, 1993.
23. Brahme A. Optimization of conformal and moving beam radiation therapy techniques. In: Bruinvis IAD, van der Giessen PH, van Kleffens HJ, eds. Use of computers in radiation therapy. Amsterdam: Elsevier, 1987: 227–30.
24. Stroom JC, de Boer HC, Huizenga H, Visser AG. Inclusion of geometrical uncertainties in radiotherapy treatment planning by means of coverage probability. Int J Radiat Oncol Biol Phys 1999; 43: 905–19.
25. Engelsman M, Damen EMF, de Jaeger K, van Ingen KM, Mijnheer BJ. The effect of breathing and set-up errors on the cumulative dose to a lung tumor. Radiother Oncol 2001; 60: 95–105.
26. Fein DA, McGee KP, Schultheiss TE, Fowble BL, Hanks GE. Intra- and interfractional reproducibility of tangential breast fields: a prospective on-line portal imaging study. Int J Radiat Oncol Biol Phys 1996; 34: 733–40.
27. Källman P, Lind BK, Brahme A. An algorithm for maximizing the probability of complication free tumor control in radiation therapy. Phys Med Biol 1992; 37: 871–90.
28. Källman P, Ågren A-K, Brahme A. Tumor and normal tissue responses to fractionated non uniform dose delivery. Int J Radiat Biol 1992; 62: 249–62.
29. Mavroidis P, Kappas C, Lind BK. A computer program for evaluating the probability of complication-free tumor control incorporated in a commercial treatment planning system. J Balkan Union Oncol 1997; 3: 257–64.
30. Ågren A-K. Quantification of the response of heterogeneous tumors and organized normal tissues to fractionated radiotherapy. Thesis. Stockholm University, 1995.
31. Lind BK, Mavroidis P, Hyödynmaa S, Kappas C. Optimization of the dose level for a given treatment plan to maximize the complication-free tumor cure. Acta Oncol 1999; 38: 787–98.
32. Withers HR, Taylor JMG, Maciejewski B. Treatment volume and tissue tolerance. Int J Radiat Oncol Biol Phys 1988; 14: 751–9.
33. Pavy JJ, Denekamp J, Letschert J, et al. Late effects toxicity scoring: the SOMA scale. Radiother Oncol 1995; 35: 11–5.
34. Steel G. Basic clinical radiobiology. UK: The Bath Press, 1997.
35. Mavroidis P, Lind BK, Van Dijk J, et al. Comparison of conformal radiation therapy techniques within the dynamic radiotherapy project 'DYNARAD'. Phys Med Biol 2000; 45: 2459–81.
36. Mavroidis P, Lind BK, Brahme A. Biologically effective uniform dose ($\bar{D}$) for specification, report and comparison of dose response relations and treatment plans. Phys Med Biol 2001; 46: 2607–30.
37. Löf J, Lind BK, Brahme A. Optimal radiation beam profiles considering the stochastic process of patient positioning in fractionated radiation therapy. Inverse Prob 1995; 11: 1189–209.
38. Brahme A. The need for accurate target and dose specifications in conventional and conformal radiation therapy. An introduction. Acta Oncol 1997; 36: 789–92.
39. Mavroidis P, Lind BK, Proimos B, Kappas C, Brahme A. Dosimetric information from films irradiated in the conformal therapy test phantom of the 'Dynarad' project. In: Kappas C, del Guerra A, Kolitsi Z, Damilakis Y, Theodorou K, eds. Medical physics. Bologna: Monduzzi Editore, 1999: 127–34.
40. Ekberg L, Holmberg O, Wittgren L, Bjelkengren G, Landberg T. What margins should be added to the clinical target volume in radiotherapy treatment planning for lung cancer? Radiother Oncol 1998; 48: 71–7.